Acknowledgements

FPW is grateful to the Faculty Research Grant for funding used to purchase telescope time. FM was supported by the NASA NY Space Grant.

References

Binzel, R.P. (1987). "A photoelectric survey of 130 asteroids." *Icarus* **72**, 135-208.

Collins, K.A.; Kielkopf, J.F.; Stassun, K.G.; Hessman, F.V. (2017). "AstroImageJ: Image Processing and Photmetric Extraction for Ultra-precise Astronomical Light Curves." *Astron. J.* **153**, 77-89.

Erasmus, N.; Navarro-Meza, S.; McNeill, A.; Trilling, D.E.; Sickafoose, A.A.; Denneau, L.; Flewelling, H.; Heinze, A.; Tonry, J.L. (2020). "Investigating Taxonomic Diversity within Asteroid Families through ATLAS Dual-band Photometry." *Astrophysical Journal Supplement Series* **247**, 13.

Hanuš, J.; Ďurech, J.; Brož, M.; Warner, B.D.; Pilcher, F.; Stephens, R.; Oey, J.; Bernasconi, L.; Casulli, S.; Behrend, R.; Polishook, D.; Henych, T.; Lehký, M.; Yoshida, F.; Ito, T. (2011). "A study of asteroid pole-latitude distribution based on an extended set of shape models derived by the lightcurve inversion method." *Astron. Astrophys.* **530**, A134.

Hanuš, J.; Ďurech, J.; Brož, M.; Marciniak, A.; Warner, B.D.; Pilcher, F.; Stephens, R.; Behrend, R.; Carry, B.; Čapek, D.; Antonini, P.; Audejean, M.; Augustesen, K.; Barbotin, E.; Baudouin, P.; and 105 authors (2013). "Asteroids' physical models from combined dense and sparse photometry and scaling of the YORP effect by the observed obliquity distribution." *Astron. Astrophys.* **551**, A67.

NASA Horizons. *https://ssd.jpl.nasa.gov/horizons/app.html#/*

Slivan, S.M. (2003). "A Web-based tool to calculate observability of Koronis program asteroids." *Minor Planet Bull.* **30**, 71-72.

Slivan, S.M.; Colclasure, A.M.; Larsen, S.S.; McLellan-Cassivi, C.J.; Neto, O.S.; Noto, M.I.; Redden, M.S.; Wilkin, F.P. (2023). "Synodic and Sidereal Rotation Periods of Koronis Family Member (1389) Onnie." *Minor Planet Bull.* **50**, 8-10.

SYNODIC AND SIDEREAL ROTATION PERIODS OF KORONIS FAMILY MEMBER (1389) ONNIE

Stephen M. Slivan, Abigail M. Colclasure, Skylar S. Larsen,
Claire J. McLellan-Cassivi, Orisvaldo S. Neto, Maurielle I. Noto,
Maya S. Redden
Massachusetts Institute of Technology,
Dept. of Earth, Atmospheric, and Planetary Sciences,
77 Mass. Ave. Rm. 54-424, Cambridge, MA 02139
slivan@mit.edu

Francis P. Wilkin
Union College Dept. of Physics and Astronomy
Schenectady, NY

(Received: 2022 October 15 Revised: 2022 October 17)

Lightcurve observations of (1389) Onnie during its 2022 apparition yield a secure determination of its synodic rotation period 23.038 ± 0.005 h, and an unambiguous count of sidereal rotations back to 2017 constrains the sidereal rotation period.

Asteroid (1389) Onnie appears to be the lowest-numbered Koronis family member lacking a secure determination of its rotation period having full lightcurve coverage and no ambiguity. Binzel (1987) recorded partial lightcurves of Onnie on three consecutive nights in 1983, each spanning about 4 to 5 hours. By assuming that either 0.5, 1.0, or 1.5 rotations elapse during the 22.5 h interval between the observed maxima, there are three candidate periods whose folded composite lightcurves are consistent with being doubly-periodic. 1.0 rotation for a 22.5 ± 0.3 h period was chosen as favored but the others could not be ruled out. Erasmus et al. (2020) refined the favored period based on ATLAS survey data "sparsely sampled" in time, but those observations share the same ~24-h cadence of the 1983 data and thus do not resolve the period ambiguity. Hanuš et al. (2011; 2013) have reported analyses of earlier sparsely-sampled data for sidereal periods and spin vectors. The new observations reported here were made with two specific objectives: to resolve the ambiguity in the rotation period (also see Wilkin et al. (2023; this issue)), and to obtain complete rotation coverage at its 2022 viewing aspect which is similar to that incompletely observed in 1983.

We observed Onnie mainly near its eastern stationary point in 2022 July to permit using the same on-chip field comparison stars over a series of nights. Nightly observing information is summarized in Table I, and instrumentation is detailed in Table II. Observations from June through August were made using telescopes at the MIT Wallace Astrophysical Observatory (WAO) in Westford, MA. Observations in September were made remotely using the CHI-2 telescope of Telescope Live in Rio Hurtado, Chile, for which the coverage was timed specifically to fill an unattractive straggler gap in rotation phase. Processing and measurement of the images were as described by Slivan et al. (2008), except that for the observations made using the smaller telescopes WAO-3 and WAO-4 the choices of synthetic aperture sizes for the on-chip relative photometry were guided by the experience of Howell (1989).

We reduced our observations for light-time and to unit distances, and for changing solar phase angle using $G = 0.23$ (Lagerkvist and Magnusson, 1990) as the slope parameter of the Lumme-Bowell model (Bowell et al., 1989). Composite lightcurves folded at the best-fitting periods corresponding to all three possible periods identified by Binzel (1987) confirm that the earlier favored solution is correct (Fig. 1) and rules out the two alias solutions (Fig. 2), noting that the alias resolution was confirmed to be insensitive to the exact choice of *G* used in the reduction. The derived synodic period 23.038 ± 0.005 h is consistent with both the less-precise result of Erasmus et al. (2020), as well as with the more-precise result of Wilkin et al. (2023; this issue) which is based on observations made in 2021.

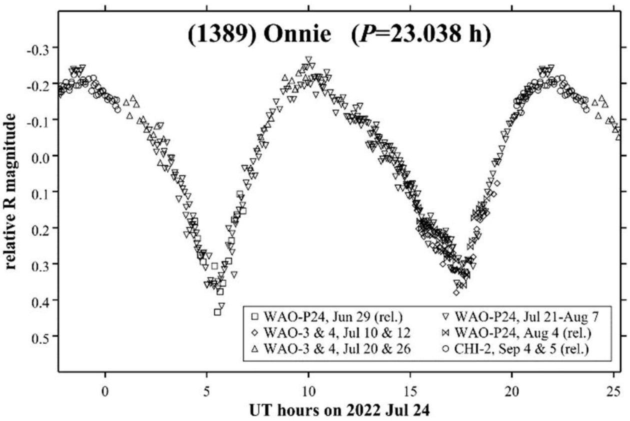

Figure 1. Folded composite lightcurve of (1389) Onnie during its 2022 apparition, light-time corrected, showing one rotation period plus the earliest and latest 10% repeated. Telescopes in the legend are identified in Table II. Lightcurves labeled "rel." were not calibrated to the same brightness zero-point as the stationary point observations; instead, they have been shifted in brightness to form a self-consistent composite.

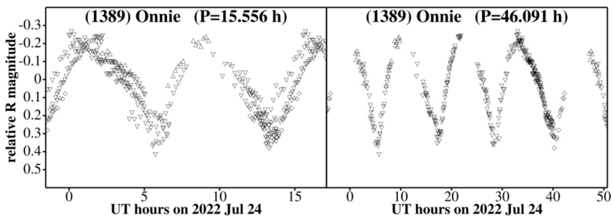

Figure 2. Similar to Fig. 1 but excluding the uncalibrated relative lightcurves, and folded at both alias periods to confirm that neither yields a self-consistent doubly-periodic composite.

In addition to the densely-sampled lightcurves from 2022 and from 2021, sparse-in-time observations made during three apparitions from 2017 to 2020 by the ATLAS astrometric survey (Tonry et al., 2018) are suitable for folded composite lightcurves and are publicly available online from the MPC astrometry Web site. The "sieve algorithm" of Slivan (2013) is used here to test whether sidereal rotations can be unambiguously counted across the combined lightcurve data set; the epochs measured for all five apparitions are given in Table III. The algorithm results (Fig. 3) confirm an unambiguous solution that corresponds to 1820.5 sidereal rotations during the maximum epoch interval, but the five apparitions from 2017 through 2022 are not sufficient to also distinguish the direction of spin, nor to unambiguously count rotations across the 27-apparition gap back to the original 1983 data. The derived sidereal period based on the epochs in Table III is constrained to be either 23.0448 ± 0.0006 h retrograde, or 23.0440 ± 0.0006 h prograde. Hanuš et al. (2011; 2013) both reported sparse-data sidereal periods of 23.0447 h with error "on the order of the last decimal place" and retrograde spin; our retrograde period agrees with theirs to within 0.0001 h.

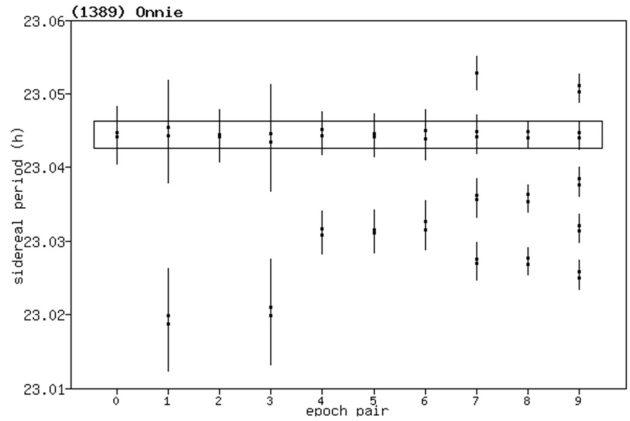

Figure 3: Single range of possible sidereal rotation periods allowed by the epochs in Table III as described in the text. The epoch measurement adopted errors are 1.5× the maximum observed asymmetry of the timing of the maxima in the corresponding composite lightcurves. Each horizontal coordinate index marks the time interval between a pair of epochs, with longer intervals to the right. Points and vertical bars represent sidereal periods and period ranges, respectively, calculated from every possible number of rotations that could elapse during the interval. The thin horizontal rectangle identifies the single range of periods that is allowed by all ten time intervals.

UT date 2022	α (°)	Tel. ID	Filter	Integration time (s)
Jun 29.3	19.8	WAO-PW	*R*	480
Jul 10.3	18.6	WAO-4	*R*	300
Jul 12.3	18.3	WAO-3	*R*	600
Jul 20.3	17.0	WAO-3	*R*	600
Jul 21.3	16.8	WAO-PW	*R*	600
Jul 22.3	16.6	WAO-PW	*R*	600
Jul 23.3	16.4	WAO-PW	*R*	600
Jul 24.3	16.1	WAO-PW	*R*	600
Jul 26.3	15.7	WAO-4	*R*	600
Jul 27.2	15.5	WAO-PW	*R*	600
Jul 31.2	14.5	WAO-PW	*R*	300
Aug 02.3	13.9	WAO-PW	*R*	300
Aug 03.2	13.7	WAO-PW	*R*	300
Aug 04.3	13.4	WAO-PW	*R*	300
Aug 07.3	12.5	WAO-PW	*R*	300
Sep 04.2	2.3	CHI-2	red	300
Sep 05.2	1.9	CHI-2	red	300

Table I: Nightly observing information, with rows grouped by lunation. Columns are: UT date at lightcurve mid-time, solar phase angle α, telescope ID (see Table II), filter (*R*, Cousins *R*; red, Astrodon Gen2 color separation red), and image integration time.

Number	Name	yyyy mm/dd	Phase	L_{PAB}	B_{PAB}	Period(h)	P.E.	Amp	A.E.
1389	Onnie	2022 06/29-09/05	19.8,1.9	346	1	23.038	0.005	0.58	0.04

Table IV. Observing circumstances and results. Solar phase angle is given for the first and last dates. L_{PAB} and B_{PAB} are the approximate phase angle bisector longitude/latitude at mid-date range.

Tel. ID	Dia. (m)	CCD camera	FOV (′)	Bin	Scale (″/pix)
WAO-3	0.36	FLI ML1001	20×20	1×1	1.18
WAO-4	0.36	SBIG STL-1001	21×21	1×1	1.25
WAO-PW	0.61	FLI PL16803	32×32	1×1	0.46
CHI-2	0.50	FLI PL16803	66×66	1×1	0.96

Table II: Telescopes and cameras information. Columns are: telescope ID (WAO-3, shed pier #3 Celestron C14; WAO-4, shed pier #4 Celestron C14; WAO-PW, Elliot PlaneWave 24-in CDK; CHI-2, ASA 500N), telescope diameter, CCD camera, detector field of view, image binning used, and binned image scale.

UT date	PAB λ (°)	Epoch (UT h)	Data ref.
2017 Oct 10	334.2	10.56 ± 1.50	a,b
2019 Jan 21	68.5	6.74 ± 1.74	a,b
2020 Mar 28	162.6	3.19 ± 1.13	a,b
2021 Apr 20	254.2	6.90 ± 0.35	c
2022 Jul 24	345.3	10.88 ± 1.31	d

Table III: Summary of lightcurve epochs, in each case locating a maximum from the second harmonic of a Fourier series model fit to the lightcurves. PAB *λ* is the J2000 ecliptic longitude of the phase angle bisector. Data references are a, ATLAS-MLO *o*-band; b, ATLAS-HKO *o*-band; c, Wilkin et al. (2023; this issue); d, this work. Photometry from the ATLAS survey (Tonry et al., 2018) was retrieved from the MPC Orbits/Observations Database.

Acknowledgements

We thank Dr. Michael Person and Timothy Brothers for allocation of telescope time at Wallace Observatory, and for observer instruction and support. The student observers were supported by a grant from MIT's Undergraduate Research Opportunities Program. F. Wilkin received funding from the Faculty Research Grant at Union College. This work also has made use of data and services provided by the International Astronomical Union's Minor Planet Center; specifically, the brightnesses accompanying astrometry from the Asteroid Terrestrial-impact Last Alert System (ATLAS) survey observing program.

References

Binzel, R.P. (1987). "A Photoelectric Survey of 130 Asteroids." *Icarus* **72**, 135-208.

Bowell, E.; Hapke, B.; Domingue, D.; Lumme, K.; Peltoniemi, J.; Harris, A.W. (1989). "Application of Photometric Models to Asteroids." In *Asteroids II* (R.P. Binzel; T. Gehrels; M.S. Matthews, eds.) pp. 524-556. Appendix: The IAU Two-Parameter Magnitude System for Asteroids. U. of Arizona Press, Tucson, AZ.

Erasmus, N.; Navarro-Meza, S.; McNeill, A.; Trilling, D.E.; Sickafoose, A.A.; Denneau, L.; Flewelling, H.; Heinze, A.; Tonry, J.L. (2020). "Investigating Taxonomic Diversity within Asteroid Families through ATLAS Dual-band Photometry." *Astrophys. J. Suppl. Ser.* **247**, A13.

Hanuš, J.; Ďurech, J.; Brož, M.; Warner, B.D.; Pilcher, F.; Stephens, R.; Oey, J.; Bernasconi, L.; Casulli, S.; Behrend, R.; Polishook, D.; Henych, T.; Lehký, M.; Yoshida, F.; Ito, T. (2011). "A study of asteroid pole-latitude distribution based on an extended set of shape models derived by the lightcurve inversion Method." *A&A* **530**, A134.

Hanuš, J.; Ďurech, J.; Brož, M.; Marciniak, A.; Warner, B.D.; Pilcher, F.; Stephens, R.; Behrend, R.; Carry, B.; Čapek, D.; Antonini, P.; Audejean, M.; Augustesen, K.; Barbotin, P.; Baudouin, P.; and 105 colleagues (2013). "Asteroids' physical models from combined dense and sparse photometry and scaling of the YORP effect by the observed obliquity distribution." *A&A* **551**, A67.

Howell, S.B. (1989). "Two-dimensional Aperture Photometry: Signal-to-noise Ratio of Point-source Observations and Optimal Data-extraction Techniques." *PASP* **101**, 616-622.

Lagerkvist, C.-I.; Magnusson, P. (1990). "Analysis of asteroid lightcurves. II - Phase curves in a generalized HG-system." *A&AS* **86**, 119-165.

Slivan, S.M.; Binzel, R.P.; Boroumand, S.C.; Pan, M.W.; Simpson, C.M.; Tanabe, J.T.; Villastrigo, R.M.; Yen, L.L.; Ditteon, R.P.; Pray, D.P.; Stephens, R.D. (2008). "Rotation Rates in the Koronis Family, Complete to $H \approx 11.2$." *Icarus* **195**, 226-276.

Slivan, S.M. (2013). "Epoch data in sidereal period determination. II. Combining epochs from different apparitions." *Minor Planet Bull.* **40**, 45-48.

Tonry, J.L.; Denneau, L.; Heinze, A.N.; Stalder, B.; Smith, K.W.; Smartt, S.J.; Stubbs, C.W.; Weiland, H.J.; Rest, A. (2018). "ATLAS: A High-cadence All-sky Survey System." *PASP* **130**, 064505.

Wilkin, F.P.; MacDonald, F.; Slivan, S.M. (2023). "Lightcurve for Koronis family member (1389) Onnie." *Minor Planet Bull.* **50**, 7-8.